European Geothermal Congress 2013
Pisa, Italy, 3-7 June 2013

DEM Study of Hydraulic Fracturing in Enhanced Geothermal Systems

Ingrid Tomac, Marte Gutierrez

Colorado School of Mines, 1500 Illinois St., Golden, CO 80401, USA

itomac@mines.edu

Keywords: enhanced geothermal systems, hydraulic fracturing, hydro-thermo-mechanical coupling, fracture tortuosity.

ABSTRACT

The paper presents results of a micro-mechanical DEM (discrete element modeling) study using the Particle Flow Code (PFC) of the hydraulic fracture initiation and propagation in enhanced geothermal systems (EGS). Hydraulic fracturing is the main means to stimulate and create flow paths to extract heat in hot dry rocks with insufficient permeability to inject and circulate fluids. Hydro-thermo-mechanical (HTM) coupled modeling is performed to analyze stress and strain changes around an injection wellbore to improve the understanding of the fracture initiation processes and the resulting fracture geometry. The study used a thermo-mechanically coupled Synthetic Rock Model (SRM) to preliminary validate previous research findings that were performed of the hydraulic fracturing in rocks but now taking into account the stresses induced by the temperature difference between fracturing fluid and the surrounding rock material. The study evaluated fracture geometry and orientation with respect to fracturing fluid temperature, viscosity, density, pressure, rock parameters and in-situ stress difference. The study used typical in-situ conditions including temperature and in situ stresses, and rock mechanical properties representative of crystalline rocks with low permeability.

1. INTRODUCTION

Hydraulic fracturing is a technique that is used for stimulation and propagation of fractures in rock mass by applying the fluid pressure. The technique was developed in the late 1940's primarily for the purposes of enhancement of oil and gas reservoirs in deep rock formations. Since the first early attempts on hydraulic fracturing, the technology has developed and its application has spread to other fields, especially to geothermal reservoirs and to waste management (Economides et al 2000). Enhanced geothermal systems (EGS) use heat from deep rock formations for steam production and electricity generation on the ground surface. Unlike conventional hydro-thermal geothermal reservoirs that use hot water and steam already available in a rock formation, EGS consists of artificially formed rock fracture systems. Therefore, the aim of hydraulic reservoir stimulation is to create a network of connected fractures that will allow for water to circulate and deliver heat back to the ground. EGS reservoirs are situated in hot dry rock (HDR) formations that consist of igneous rocks such as granite. EGS are gaining more and more attention in order to be used as a sustainable source of energy. The implementation of the hydraulic fracturing to produce the long-term functional geothermal reservoir is still a challenge.

The motivation for this research is better understanding of hydro-thermo-mechanical processes related to hydraulic fracturing of hot dry rocks in (EGS). Besides being very deep (typically 2 to 5 km in depth) and under high in-situ stresses, temperature of the rock mass can exceed 200°C (Tester et al 2006). However, fracturing fluid has usually a lower temperature than the surrounding rock mass. In spite of theoretica (Schmitt and Zoback 1993) and other models (Kristianovic and Zheltov 1955, Perkins and Kern 1997, Yew 1997, Clifton and Wang 1988) that are currently used for hydraulic fracturing prediction, the effect of induced thermal stresses on hydraulic fracture initiation and propagation is not completely understood and incorporated in those models.

The objectives of this study are to build a computational model that will be able to capture hydro-thermo-mechanical behaviour of granite during hydraulic fracturing. Particularly, the effect of convective heat transfer with fracturing fluid and conductive heat transfer on fracture propagation, micro-fractures and tortuosity around the wellbore is studied.

2. HYDRO-THERMO-MECHANICAL MODEL

The hydro-thermo-mechanical model is built using the Discrete Element Code PFC^{2D} (Particle Flow Code) (Itasca 2004). The model incorporates coupling of hydraulic fracturing, fluid flow in a fracture, heat convective fluid flow and conductive heat flow within a rock mass. Non-linear stress-strain rock response means that new fractures are formed in the DEM rock matrix. A DEM model consists of discrete disk particles with out-of-plane dimension of one. Mechanical stress-strain response follows a bonded-particle model (BPM) that is used to model rock mass (Potyondy and Cundall 2004) . Change in stresses and strains are updated during mechanical time-stepping,

as well as fracture propagation that is related to bond breakage and separation of particles. Thermal transient heat conduction logic is coupled with mechanical behavior of DEM through individual particles volume change associated with particle temperature change and corresponding material properties. The heat flow through rock mass is calculated during thermal time-steps framework. The thermal time is then stopped while a mechanical time-stepping procedure is executed. The heat flow between particles that are not in contact is disabled (Itasca 2004). The thermal DEM option introduces thermal pipes between adjacent particles and reservoirs that are positioned at the particle center of mass. The conductive heat flow occurs in active pipes that connect heat reservoirs within the DEM particles assembly. Under assumption that the strain changes play a negligible role in influencing the temperature, the heat conduction equation for a continuum is:

$$-\frac{\partial q_i}{\partial x_i} + q_v = \rho C_v \frac{\partial T}{\partial t} \qquad [1]$$

where q_i is the heat-flux vector (W/m^2), $\partial q_i / \partial x_i$ is the heat-flux gradient in the pipe (x represents a direction of the pipe along its length), q_v is the volumetric heat-source intensity or power density (W/m^3) of the reservoirs connected with the pipe, ρ is the mass density of the particle (material), C_v is the specific heat at constant volume (J/(kg^{0}C)), T is the temperature (^{0}C) and t is time. Thermally induced strains are obtained as a consequence of particle radii modification caused by the temperature changes, and the force carried in each parallel bond accounts for heating of both particle and the bonding material. A thermal pipe is associated with each particle-particle contact, and becomes automatically active if the particles overlap at the contact or if the parallel bond is present between two particles. The relation between the heat-flux and the temperature gradient is (Fourier law):

$$q_i = -k_{ij} \frac{\partial T}{\partial x_j} \qquad [2]$$

where k_{ij} is the thermal conductivity tensor (W/(m^{0}C) and $\partial T / \partial x_j$ is the temperature gradient in the pipe. Boundary and initial conditions are applied on particles (temperature reservoirs). Numerical discretization of equation [1] is given for a system of thermal pipes and reservoirs. The Gauss-Ostrogradsky's divergence theorem is used as a basis for describing heat flow from one reservoir to another, using the pipes network. Control volumes, or reservoirs, are situated in the center of each particle. The sum of all reservoir volumes in this scheme is equal to the material volume. Integrating the field's divergence over the interior of the single heat reservoir equals the integral of the vector field over the reservoir's boundary. The heat flow per unit volume of particle can be developed as:

$$\frac{\partial q_i}{\partial x_i} = \frac{1}{V}\int_V \frac{\partial q_i}{\partial x_i} dV = \frac{1}{V}\int_S q_i n_i dS = \\ = \frac{1}{V}\sum_{p=1}^{N} q_i^p n_i^p \Delta S^p = \frac{1}{V}\sum_{p=1}^{N} Q^p \qquad [3]$$

where q_i is the heat-flux vector, x_i is the length along the pipe, V is the heat reservoir control volume, S is the surface of the control volume, n_i is the outward unit normal vector of the surface, p is the heat flow pipe, N is the number of heat flow pipes for each control volume and Q^p is the power in pipe p that is flowing out of the reservoir. The heat conduction equation for a single reservoir is found by substitution of equation [3] into equation [1]:

$$-\sum_{p=1}^{N} Q^p + Q^v = mC_v \frac{\partial T}{\partial t} \qquad [4]$$

where Q_v is the heat-source intensity, m is the thermal mass, C_v is the specific heat at constant volume. Each pipe is regarded as a one dimensional object with a thermal resistance per unit length of η, then the power is given by:

$$Q = -\frac{\Delta T}{\eta L} \qquad [5]$$

where ΔT is the temperature difference between the two reservoirs at each end of the pipe, and L is the pipe length. The time derivative of heat flow from equation [4] can now be calculated using forward finite differences:

$$\frac{\partial T}{\partial t} = \frac{1}{mC_v}\left[-\sum_{p=1}^{N} Q^p + Q^v\right] = \frac{1}{mC_v}\tilde{Q} \qquad [6]$$

where $\tilde{Q}$ is the out-of-balance power. Starting with an initial temperature field at particles, the power in each pipe is updated using equation [5]. Then, reservoir temperature is updated using the forward difference expression:

$$T_{t+\Delta t} = T_t + \Delta T = T_t + \Delta t\left(\frac{1}{mC_v}\tilde{Q}\right)_t \qquad [7]$$

where Δt is the thermal time-step. Thermal strains in PFC^{2D} are obtained from the thermal expansion of the particles and the parallel bond. The particle radius change is:

$$\Delta R = \alpha R \Delta T \qquad [8]$$

where R is the particle radius, α is the coefficient of linear thermal expansion associated with the particle and ΔT is the temperature change. If the parallel bond is present at the contact associated with the pipe, the normal component of the force vector carried by the bond will be affected by the temperature change. An isotropic expansion of the bond material changes the bond length. This is modeled by changing the normal component of the bond force vector as:

$$\Delta \bar{F}^n = -\bar{k}^n A \Delta U^n = -\bar{k}^n A(\bar{\alpha}\bar{L}\Delta T) \quad [9]$$

where $\Delta \bar{F}^n$ is the force vector in the bond, $\bar{k}^n$ is the bond normal stiffness, A is the area of the bond cross-section, $\bar{\alpha}$ is the expansion coefficient of the bond material, $\bar{L}$ is the bond length and ΔT is the temperature increment (equal to the average temperature change of the two particles at the ends of the pipe associated with the bond).

For the purpose of hydraulic fracturing of the BPM, additional model elements are introduced in order to couple fluid and rock, and obtain the fracture propagation in the form of broken parallel bonds. For the solid material of low porosity, such as BPM, the flow pathways may be assumed to consist of parallel-plate channels at contacts. The aperture of such a channel is proportional to the normal displacement at corresponding contacts. In the case of bonded material, the channel opening will not increase from its initial value unless the bond is broken, and the adjacent particles distance increases. In addition to flow channels, fluid reservoirs are modeled as finite fictive volumes between particles that connect flow channels. The flow rate in a channel is given by:

$$q = \frac{a^2}{12\mu}\frac{(P_2 - P_1)}{L} \quad [10]$$

where q is the flow rate, μ is the fluid dynamic viscosity, and P_2-P_1 is the pressure difference between the two adjacent domains, L is the channel length equal to the harmonic sum of adjacent particles radii and a is the channel aperture. Each reservoir receives flows from the surrounding channels. In one time-step the increase in fluid pressure is given by the following equation, assuming that inflow is taken positive:

$$\Delta P = \frac{K_f}{V_d}\left(\sum q\Delta t - \Delta V_d\right) \quad [11]$$

where K_f is the fluid bulk modulus, V_d is the apparent volume of the reservoir, and Δt is the time-step. Reservoir pressure exerts tractions on the enclosing particles, which are transferred to the particle through the assumed polygonal path that joins contacts that surround a reservoir. The force vector on a typical particle is:

$$F_i = P n_i s \quad [12]$$

where F_i is the force on particle, P is the reservoir pressure, n_i is the unit vector in direction of the particle, s is the length between two contacts.

Heat is convected with fluid flow through channels in rock matrix, and particle temperature is updated after each mechanical time-step. Thermal coupling between fluid and particle is modeled as a thermal input parameter T_p. Temperatures of particles next to fluid channels are updated to represent a new fracture surface boundary condition for rock matrix at next thermal time-step. Boundary condition for convective heat flow in the channel between two surfaces is introduced as the average temperature of adjacent particles. The heat convection model in fracture is built with several assumptions. First, the advective heat transfer is assumed along the length of the channel. Second, a fully developed fluid velocity profile in the channel underlies the heat convection. Conductive heat flow in the fluid along the channel length is neglected. Potential and kinetic energy changes are neglected in calculation. The fluid specific heats and overall heat transfer coefficient are constant. Convection solution for each channel is modeled for a steady-state within each mechanical time-step and with corresponding boundary conditions at the beginning of the time-step. First, it is assumed that under laminar conditions and low Reynolds and Prandtl flow numbers, the entrance region for each channel is small, and the convective heat transfer is modeled for fully developed heat transfer profile (Fig. 1).

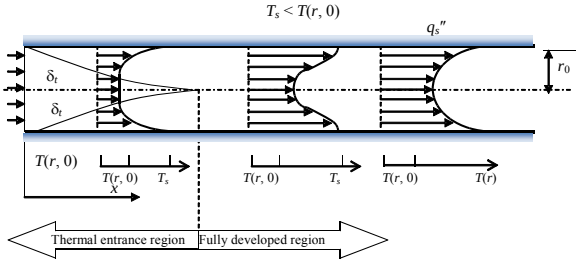

Figure 1: Development of a thermal boundary layer in a heated channel

When fluid enters a circular tube with a cross-section radius r, at a uniform temperature, $T(r,0)$ that is less than the pipe surface temperature, T_s, a convection heat transfer occurs and a thermal boundary layer begins to develop. After some time, at the moment t and position $x_{fd,t}$ and a thermally fully developed condition is eventually reached. For fully developed flow in a pipe, mean velocity and mean temperature parameters are introduced. The mean (bulk) temperature of the fluid at a given cross section is defined in terms of the thermal energy transported by the fluid as it moves past the cross-section. As fluid flows with a constant velocity along the pipe axis, it gets heated. Hence, the term mean temperature of the fluid is introduced as:

$$\frac{\partial}{\partial x}\left[\frac{T_s(x) - T(r,x)}{T_s(x) - T_m(x)}\right]_{fd,t} = 0 \quad [13]$$

where x is the axial pipe dimension, $T_s(x)$ is the pipe surface temperature at a position x along the pipe, $T_m(x)$ is the mean pipe temperature at a position x along the pipe, and $T(r,x)$ is the fluid temperature at a position x along the pipe and distance r from the center of the pipe in y direction perpendicular to x. The expression for a mean temperature variation along the pipe for a mean temperature $T_{m,out}$ is in the case of

constant pipe surface T_s temperature is derived from the energy balance for a control volume:

$$\frac{T_s - T_m(x)}{T_s - T_{m,i}} = e^{\left(-\frac{Px}{\frac{dm}{dt}}\bar{h}\right)} \quad [14]$$

where T_s is the pipe temperature surface, $T_{m,i}$ is the fluid temperature at the entrance of the pipe, $T_m(x)$ is the mean pipe temperature at a position x along the pipe, P is the pipe perimeter ($P=\pi D$ where D is the pipe diameter), dm/dt is the fluid mass flow rate through the pipe cross-section at position x and $\bar{h}$ is the average value of h for the entire tube length. The average heat convection coefficient can be derived using the Nusselt number for a laminar flow in a circular tube ($N_{uD}=hD/k_f=3.66$ for constant T_s) [9]. The transient solution to the heat transfer problem is obtained using the conservation of energy. At each fixed volume, and at any time, there must be a balance of all the energy rates involved in the problem, measured in joules per second (W). If the inflow energy equals the outflow, a steady-state condition must prevail in which there will be no change in the amount of energy stored in the control volume:

$$\frac{dE_{in}}{dt} - \frac{dE_{out}}{dt} = \frac{dE_{st}}{dt} \quad [15]$$

where dE_{in}/dt is the rate of change of inflow energy, dE_{in}/dt is the rate of change of outflow energy and dE_{st}/dt is the rate of change of energy stored in the control volume.

Energy conservation requirement (equation 15) is applied to a differential control volume in the thermal boundary layer. Neglecting potential energy effects, the energy per unit mass of the fluid includes the thermal internal energy e and the kinetic energy $v^2/2$ and $v^2=v_x^2+v_y^2$. Accordingly, using Eulerian approach, thermal and kinetic energy are advected with the bulk fluid motion across the control surfaces, and for the x direction, the net rate at which this energy enters the control volume is:

$$\frac{dE_{adv,x}}{dt} - \frac{dE_{adv,x+\Delta x}}{dt} = -\frac{\partial}{\partial x}\left[\rho v_x\left(e+\frac{v^2}{2}\right)\right]dxdy \quad [16]$$

where $dE_{adv,x}/dt$ is the energy advection rate, ρ is the fluid density, v_x is the average fluid velocity in x direction at a control volume, ν is the fluid kinematic viscosity, e is the thermal internal energy per unit mass. Energy is also transferred across the control surface by molecular processes, namely by a conduction energy transfer. For the conduction process, the net transfer of energy into the control volume is:

$$\frac{dE_{cond,x}}{dt} - \frac{dE_{cond,x+\Delta x}}{dt} = \frac{\partial}{\partial x}\left(k\frac{\partial T}{\partial x}\right)dxdy \quad [17]$$

where $dE_{cond,x}/dt$ is the energy conduction rate, k is the thermal conductivity constant, and T is the temperature.

Adding those equations in x and y direction, and neglecting viscous dissipation term (fluid friction that is turned to thermal energy) and neglecting the energy generation rate at control volume from other sources, the following thermal energy equation can be derived for control volume and incompressible fluid for the steady-state flow:

$$\rho c_p\left(v_x\frac{\partial T}{\partial x} + v_y\frac{\partial T}{\partial x}\right) = \frac{\partial}{\partial x}\left(k\frac{\partial T}{\partial x}\right) + \frac{\partial}{\partial y}\left(k\frac{\partial T}{\partial y}\right) \quad [18]$$

If transient flow is considered, some amount of energy storage will be included at each time t in the control volume of the fluid (equation 17), and it can be written as:

$$\frac{dE_{st}}{dt} = \frac{d}{dt}(\rho VcT) \quad [19]$$

Now we can write the transient flow energy conservation equation for the control volume:

$$\rho c_p\left(v_x\frac{\partial T}{\partial x} + v_y\frac{\partial T}{\partial x}\right) - \frac{\partial}{\partial x}\left(k\frac{\partial T}{\partial x}\right) + \\ + \frac{\partial}{\partial y}\left(k\frac{\partial T}{\partial y}\right) = \frac{d}{dt}\left(\rho Vc_vT\right) \quad [20]$$

where T is the temperature, v_x and v_y are fluid velocities, ρ is fluid density, k is the Boltzmann's constant, t is time, c_v is the specific heat at constant volume, c_p is the specific heat at constant pressure.

A change in energy storage for each mechanical time-step will be introduced in the fluid reservoir domain, and the heat-flux from the domain will be introduced to the rock mass as a boundary condition for thermal time-step calculation.

The rate at which convective heat transport occurs along the pipe may be obtained by integrating the product of the mass flux and the internal energy per unit mass over the cross-section:

$$\frac{dE_t}{dt} = \int_{A_c} \rho v_x c_v T dA_c \quad [21]$$

Hence, if mean temperature T_m for a pipe cross-section is used, equation 21 can be written as:

$$\frac{dE_t}{dt} = \frac{dm}{dt}c_vT_m \quad [22]$$

At each fluid domain, a control change in volume is assigned through the fluid flow FISH function. Accordingly, the conservation of energy can be written for a domain. The change in the domain thermal energy storage is equal to the heat flow rate from the adjacent pipes minus the thermal energy of the domain at the beginning of the time-step:

$$\Delta E_{dom} = E_t - E_{dom} \qquad [23]$$

where E_{dom} is the domain thermal energy and E_t is the convective heat transfer from the adjacent fluid pipes. Combining equations 19, 22 and 23, the domain temperature change due to the convective transport with fluid through pipes can be derived as:

$$\Delta T_{dom} = \frac{\Delta t}{\rho \Delta V c_p}\left[\sum_{p=1}^{N} \rho v_p \pi a_p^2 c_v T_{m,L} - T_{dom}\right] \qquad [24]$$

where ΔT_{dom} is the temperature change in fluid domain, ΔV is fluid domain volume, ρ is fluid density, k is the Boltzmann's constant, t is time, c_v is the specific heat at constant volume, c_p is the specific heat at constant pressure, and $T_{m,L}=T_m(x)$ for $x=L$ where L is the length of the pipe, is the mean temperature at the end of the pipe (equation 23).

The change in local boundary condition at the fracture surface due to the convective heat flow reflects as an updated particle temperature for the next thermal time-step:

$$T_p = T_p - \frac{\Delta T_{dom} \Delta t}{\rho r_p C_v} \qquad [25]$$

where C_v is the specific heat at constant volume, r_p is the particle radius, ρ is the particle density, Δt is mechanical time-step, ΔT_{dom} is the change in fluid reservoir temperature, T_{dom} is the change in fluid reservoir temperature, T_p is the particle temperature.

2.1. Thermal and mechanical time-stepping

The PFC^{2D} scheme manually alternates between thermal and mechanical time-stepping. Hydraulic fracture propagation is typically very fast (hundreds of m/s), while the thermal changes in rock occur more slowly. Recently, Huang (2013) presented a thermo-mechanical conductive model for hydraulic fracturing. In this paper, both the development of crack patterns and the concomitant evolution of stress and temperature fields were successfully predicted and comparison was made with theoretical models.[10] The paper proposed that by taking the time required for a diffusive thermal front to travel a distance represented by a minimum possible crack size in the system and thermal diffusivity of rock mass, it is possible to estimate maximum allowable thermal time-step. The mechanical time-step in PFC^{2D} is determined from the pressure wave propagation estimation in the system. Thermal time-step is related to mechanical time-step in a way that it represents a portion of time required for thermal flux to travel the small distance represented by the average particle size multiplied by the mechanical time-step.

3. RESULTS

Preliminary results are shown for hydraulic fracturing of granite block with three different fracturing fluids. Initial rock temperature was set to 250 °C, and fracturing fluids temperatures were 50 °C and 200 °C. Tables 1 and 2 show chosen micro and macro-parameters that describe physical, mechanical and thermal properties of rock mass and fracturing fluid. Dimensions of the model are 30 x 60 cm^2 for Model I 80 x 80 cm^2 for Model II, and confinement stresses are $\sigma_{h,min}$=4.0 MPa and $\sigma_{v,max}$=6.0 MPa.

Table 1: Rock mass micro-parameters, R_{min} is the minimum particle diameter, R_{max} is the maximum particle diameter, k_n is the normal stiffness of the particle, k_n is the shear stiffness of the particle, Pb_k_n is the normal stiffness of the parallel bond, Pb_k_s is the shear stiffness of the parallel bond, *Pb_nstr* is the normal strength of the parallel bond, *Pb_sstr* is the shear strength of the parallel bond, C_v is the specific heat at constant volume of the particle, α_t is the thermal resistance per unit length, k is the thermal conductivity of rock, Δt_{mech} is the mechanical time-step and Δt_{therm} is the thermal time-step.

Synthetic rock mass parameters in PFC^{2D}	
R_{min} (mm)	2.0
R_{max} / R_{min}	1.66
k_n (GPa)	60.0
k_s (GPa)	24.0
Pb_k_n (GPa)	$40.1 \cdot 10^3$
Pb_k_s (GPa)	$16.04 \cdot 10^3$
Pb_nstr (MPa)	8.0
Pb_sstr (MPa)	200.0
Pb_r (-)	1.0
C_v (J/kg°C)	1015.0
α_t (1/°C)	$3.711 \cdot 10^{-6}$
k (W/m°C)	2.5
Δt_{mech} (s)	10^{-5}
Δt_{therm} (s)	10^{-6}

Table 2: Fracturing fluid parameters, ρ is the mass density of fluid, μ is the dynamic fluid viscosity, T is the fluid temperature, C_v is the specific heat at constant volume of fluid.

Fracturing fluid	
ρ (kg/m^3)	1000.0
μ (Pa·s)	0.0001-0.01
T (°C)	50.0-200
C_v (J/kg°C)	3000

Hydraulic fracturing is initiated with a constant fluid pressure in the wellbore. The fracture propagation stopped after a while, because of stress dissipation.

For further fracture propagation in this model, pressure in the wellbore needs to be manually adjusted. It would be more appropriate to introduce a constant flow rate in the wellbore to control fracturing, and this is one of the further plans to develop this

Figures 2 and 3 show preliminary results of hydro-thermo-mechanical behavior of homogeneous rock mass around the wellbore. Figure 2 shows results with fluid temperature T_f=200 °C. Pressure in the wellbore was increased in stages to allow for fracture to propagate. Number of cracks (N) was monitored and heat flux was measured (q) for fracturing with different fluid dynamic viscosities (μ). In all cases presented on Figures 2 and 3, the initial rock permeability was set to zero. Fracturing form the wellbore is initiated and fracture is propagated in the direction of maximum confining stresses. It can be seen that convective heat flow causes cooling of rock matrix around the fracture. However, secondary fractures that might occur and be caused by local rock cooling were not observed. The dimensions of model and especially hydraulic aperture of fracture in this model are relatively small, and the substantial cooling of rock mass was not observed during the short time of fracture propagation (milliseconds). The specific heat at constant volume and pressure for fracturing fluid was set the same, and as a value that corresponds to the water (Table 2).

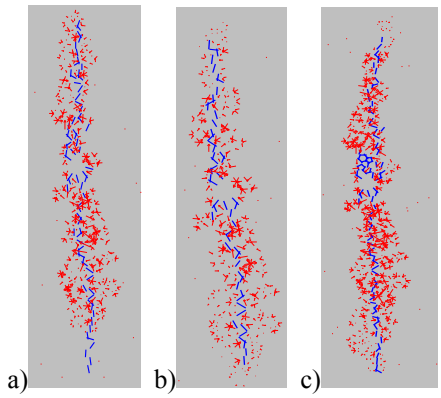

Figure 2: Fracture propagation Tf=200 °C, a) μ=0.000001 Pa·s, N=68, q=9.6·10-2 W/m2, b) μ=0.0001 Pa·s, N=52, q=6.1·10-2 W/m2, c) μ=0.01 Pa·s, N=88, q=1.0·10-1 W/m2

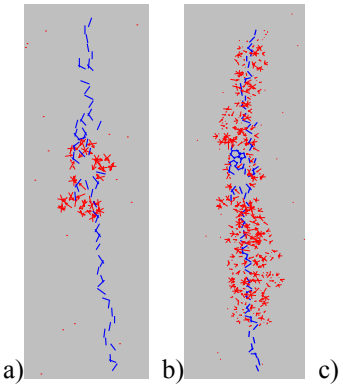

Figure 3: Fracture propagation T_f=50 °C, a) μ=0.000001 Pa·s, N=61, q=1.3·10^{-2} W/m^2, b) μ=0.0001 Pa·s, N=90, q=9.9·10^{-2} W/m^2, c) μ=0.01 Pa·s, N=63, q=4.8·10^{-2} W/m^2

Thermal fracturing of the rock mass around the wellbore was observed in DEM study by keeping the borehole fluid at a constant temperature, but stagnant without applied pressure. Figure 4 shows micro-fractures around wellbore. There is a scattered semi-circular fractured zone around the wellbore. Single fractures that propagate away from the wellbore were not observed in this case.

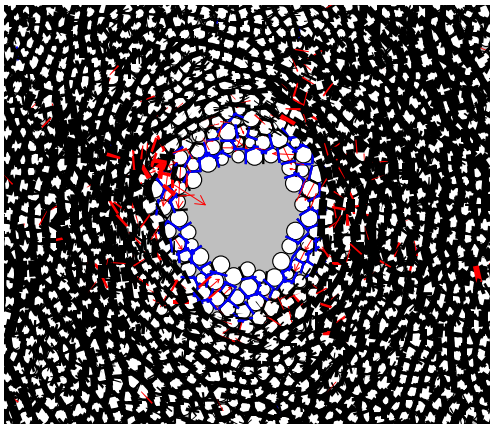

Figure 4: Thermal fracturing around the wellbore, t=40 s, T_f=10 °C

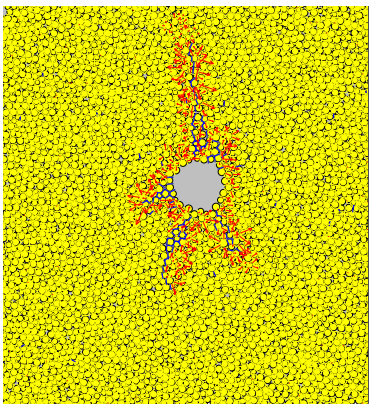

Figure 5: Fracturing of 80 x 80 cm sample, t=0.012 s, P=17 MPa, T_f=20 °Cq=2,5·10-4 W/m^2

Figure 5 shows the result of confined specimen hydraulic fracturing simulation, when the rock permeability is set to zero. Blue micro-fractures show broken tensile parallel bonds between DEM particles, and red arrows represent heat flux in rock mass. Since heat flow is very slow in comparison to the fracture propagation, the fracture surface is cooled but thermal stresses are not sufficient to produce secondary thermal fractures. Permeability of the rock matrix enhances the convection of fluid through micro-pores and channels. As a result, the rock mass is cooled faster around the wellbore, causing more extensive thermal micro-fracturing. An example calculation with permeable rock mass is shown on Figure 6. The parameter for granite micro-permeability in DEM was

taken the same as in previously reported study [11]. Rock mass around the wellbore is mechanically fractured, but due to heat flow between pores, temperature distribution is different.

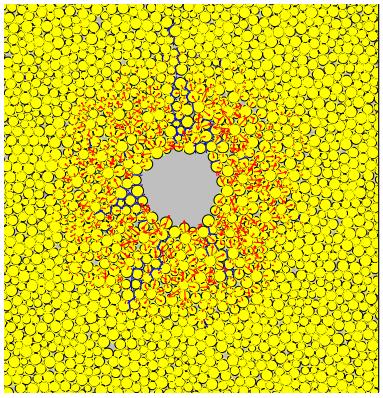

Figure 6: Fracturing of 80 x 80 cm sample, t=0.002 s, P=17 MPa, T_f=20 °C q=2,5·10-6 W/m^2

Results with a model that contains rock porosities are preliminary (Figure 6). They follow an assumption of pores saturated with fluid, but fluid is not pressurized with confinement stresses. On the contrary, in the underground rock mass, fluid in pores would be under pressure, as well. When the stresses change in the rock mass, pore pressure responses by taking a portion of stress until the excess pore pressures dissipate with time. Behavior of rock mass under confinement and subjected to hydraulic fracturing behaves like unsaturated media, because the speed of fracture propagation is very fast compared to dissipation of pore pressures. The rock response needs to be modeled with more accuracy, using poroelasticity.

4. CONCLUSIONS

The results of the study presented in this paper show the importance of accurate modelling a short-term rock mass response. The DEM model developed takes into account hydro-thermo-mechanical stress and strain propagation during hydraulic fracturing. Heat convection is combined with fluid flow in the fracture during hydraulic fracture propagation. Change in fluid temperature in fracture and heat transfer from fluid to the fracture surface is coupled with conductive response of rock mass itself.

Representation of initial rock mass permeability is only roughly taken into account, without ability of water in pores to transfer normal stresses. Stresses are transferred through a rock mass only with particles contacts and their parallel bonds. This shortcoming of the model needs to be updated by introducing poroelasticity.

Effect of thermal stresses at the tip of hydraulic fracture depends on the initial permeability of the rock mass. In the case of zero permeability in numerical simulation, convection with fluid flow in fracture was a dominant heat transfer mechanism. Fluid flows through newly formed fracture in the direction of maximum confined stress. However, when the rock matrix permeability was increased, heat flow was both convected and conducted in all directions symmetrically around the wellbore, choosing small passages of fluid that was flowing through existing micro-cracks around the wellbore.

REFERENCES

1. Economides, M. J., Nolte, K. G.: Ahmed, U., Reservoir stimulation, *Wiley* (2000).
2. Tester, J. W., Anderson, B., Batchelor, A., Blackwell, D., DiPippo, R., Drake, E., Garnish, J., Livesay, B., Moore, M. C.; Nichols, K., The future of geothermal energy: Impact of enhanced geothermal systems (EGS) on the United States in the 21st century, *Massachusetts Institute of Technology, DOE contract DE-AC07-05ID14517 final report* (2006).
3. Schmitt, D. R., Zoback, M. D: Infiltration effects in the tensile rupture of thin walled cylinders of glass and granite: Implications for the hydraulic fracturing breakdown equation, *International journal of rock mechanics and mining sciences & geomechanics abstracts*, Elsevier, pp. 289-303 (1993).
4. Khristianovic, S., Zheltov, Y.: Formation of vertical fractures by means of highly viscous fluids, *In Proceedings of 4th World Petroleum Congress*, Rome, Italy, pp 579-586 (1955).
5. Perkins, T.; Kern, L.: Widths of hydraulic fractures. *Journal of Petroleum Technology*, **13**, 937-949 (1961)
6. Yew, C. H.: Mechanics of hydraulic fracturing, *Gulf Professional Publishing*, (1997).
7. Clifton, R., Wang, J: Multiple fluids, proppant transport, and thermal effects in three-dimensional simulation of hydraulic fracturing, *In Proceedings of SPE Annual Technical Conference and Exibition*, Huston, Texas, (1988).
8. Potyondy, D., Cundall, P.: A bonded-particle model for rock, *International journal of rock mechanics and mining sciences*, **41**, 1329-1364 (2004).
9. Bergman, T. L., Incropera, F. P., Lavine, A. S., DeWitt, D. P.: Fundamentals of heat and mass transfer. *John Wiley & Sons*, (2011).
10. Huang, H., Plummer, M., Podgorney, R.: Simulated evolution of fractures and fracture networks to thermal cooling: A coupled discrete element model and heat conduction model, *In Proceedings of Thirty-Eighth Workshoop on Geothermal Resrvoir Engineering Stanford University*, Standford (2013).
11. Shimizu, H., Murata, S., Ishida, T.: The distinct element analysis for hydraulic fracturing in hard rock considering fluid viscosity and particle size distribution. *International Journal of Rock Mechanics and Mining Sciences*, **48**, 712-727, (2011)

Acknowledgements

Financial support provided by the U.S. Department of Energy under DOE Grant No. DE-FE0002760 is gratefully acknowledged. The opinions expressed in this paper are those of the authors and not the DOE.